TEM Journal. Volume 5, Issue 3, Pages 253-262, ISSN 2217-8309, DOI: 10.18421/TEM53-01, August 2016.

# About the Effectiveness of Several Dissimilarity Estimators used in Damage Assessment

Vasile Iancu [1], Gilbert-Rainer Gillich [1], Cristian Paul Chioncel [2]

[1]*Department of Mechanics, "Eftimie Murgu" University of Resita, Romania*
[2]*Department of Electrical Engineering, "Eftimie Murgu" University of Resita, Romania*

***Abstract* – This paper introduces a robust method for vibration-based damage assessment, which is based on a mathematical relation contrived by the authors that involves the frequency shifts, the damage size and position. Databases containing damage indicators for all possible damage scenarios, for three types of beams, were developed by involving this mathematical relation. The proposed damage indicator is expressed using the relative frequency shifts. The damage location and severity can be assessed if the relative frequency shifts are derived from measurements at the initial state and periodically afterwards. The paper investigates the effectiveness of several dissimilarity estimators, to find damage involving frequencies measured without and in the presence of noise.**

***Keywords* – Euler-Bernoulli beam, damage assessment, natural frequency, dissimilarity estimation.**

## 1. Introduction

For the most mechanical, civil and aerospace structures, the maintenance costs are frequently among the largest expenditures. Ageing of structures can lead to downtime or even to collapse, in this last case the structure becomes a hazard for its users. The ability to evaluate the structural integrity and discover damage at an early stage, before it can harm the structure, can significantly reduce these costs [1].

DOI: 10.18421/TEM53-01
https://dx.doi.org/10.18421/TEM53-01

**Corresponding author:** Gilbert-Rainer Gillich
Department of Mechanics, "Eftimie Murgu" University of Resita, Romania
**Email:** gr.gillich@uem.ro



A lot of the global damage assessment methods are vibration-based, the state of the structure being investigated using its vibration response. The natural frequency is the most relevant feature while it is acquired with common equipment and it characterizes the structure at once, thus the necessity of numerous measurement points being avoided [2,3]. At the use of natural frequencies the main issue is the lack of sensitivity to damage, noise sensitivity and difficulties to precisely estimate the frequency from the measured time signals. If model-based methods are employed, the errors in the model can exceed the frequency changes due to damage [4-6]. In addition, loads due to operational conditions or environment may alter the structural behavior and indicate false damages, or can even mask the damage [7]. Monitoring methods based on the mode shapes or curvatures also represent alternatives, but in the opinion of the authors, these features are difficultly achievable and imply numerous sensors [8-10].

The method presented in this script allows a precise location and severity evaluation of cracks by comparing the damage indicator attained from measurements with all possible damage patterns defined analytically or by finite element analysis (FEA). Here, the method is applied and demonstrated for the detection of open cracks in beams with three different boundary conditions. The fit between the damage indicator and the most appropriate pattern, indicating the damage depth and location, is performed by using three dissimilarity estimators: the Minkowski distance, the Histogram intersection and the Kullback-Leibler divergence. This study aimed to find a proper estimator, able to indicate the damage location and severity, even if the natural frequencies are inaccurately acquired.

## 2. Background

In this section, we present the vibrational behavior of a continuous beam in the healthy state and in the presence of damage. The structural analysis is firstly performed by means of FEA. The specimen consists of a prismatic steel beam with the

length $L$ = 1000 mm, the cross-section base b=50 mm and the cross-section height $h$=5 mm. The volumetric mass density of the specimen is $\rho$=7850 kg/m$^3$, the Young's modulus $E$=2·1011 N/m$^2$ and the Poisson's ratio $\upsilon$=0.3. To illustrate the method's versatility, and meanwhile test the dissimilarity estimators in various conditions, three support cases are considered. These cases include the classical boundary conditions that are: free end, fixed end and pinned. Namely, the beams have fixed-free, fixed-fixed respectively simply supported ends. An example of this last case is presented in Fig. 1.

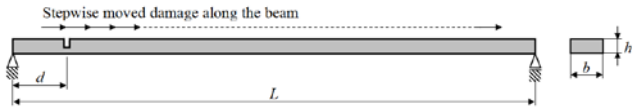


*Figure 1. Simply supported beam with the damage removed stepwise*

The ANSYS software has been employed to perform the modal analysis. Hexahedral elements with the maximum imposed edge of 1 mm were used in order to attain the frequency values with high accuracy. Among the achieved frequencies, these corresponding to the weak-axis bending modes are selected and used as a benchmark in the damage detection process.

In the three beams, failures in form of open cracks have been created. We preferred this type of damage, because of the complexity induced by it in the beam behavior. To get a complete image about the effect of damage on the natural frequencies, we took in consideration cracks with eight depth levels and successively relocated each crack in around of 200 different positions along the beam. In all cases the damage width was maintained as $w$=2 mm. The eight levels of the crack depth were: $a_1$=0.4 mm; $a_2$=0.85 mm; $a_3$=1.25 mm; $a_4$=1.65 mm; $a_5$=2.1 mm; $a_6$=2.5 mm; $a_7$=2.9 mm; $a_8$=3.35 mm. The distance between two successive locations does not exceed 10 mm. We created 3 databases from almost 4800 damage scenarios, each one characterized by the beam type and involving eight depth levels. Fig. 2.(a) to (c) illustrates the attained frequency shifts for the first three bending modes of the analyzed beams, occurred due to an open crack of depth 1.25 mm. These curves, nominated as the frequency shift curves, allow a comprehensive view on the databases.

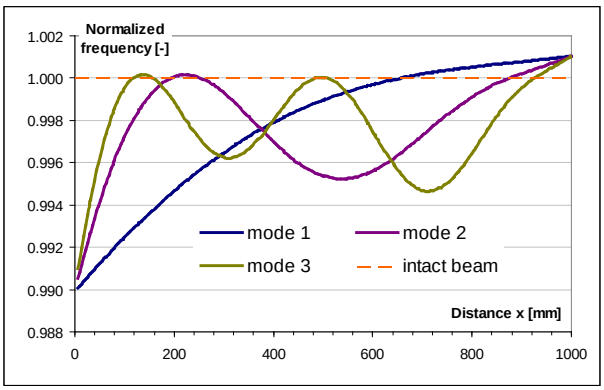


*(a)*

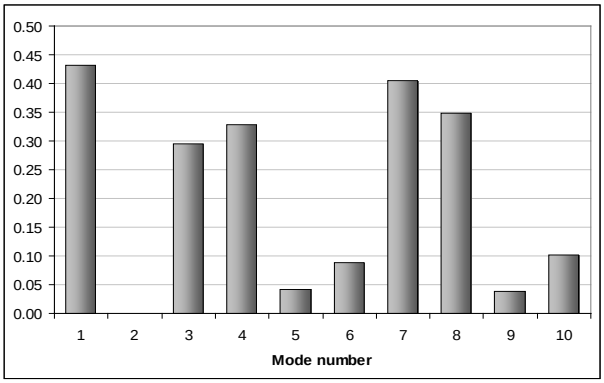


*(b)*

*Figure 2. (a) Frequency shift curves and (b) RFSs for the cantilever beam damaged at x=254mm*

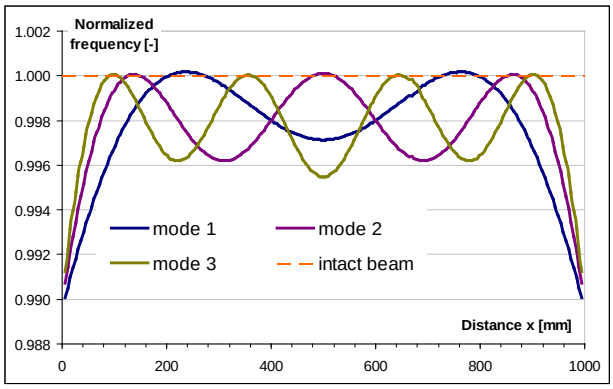


*(a)*

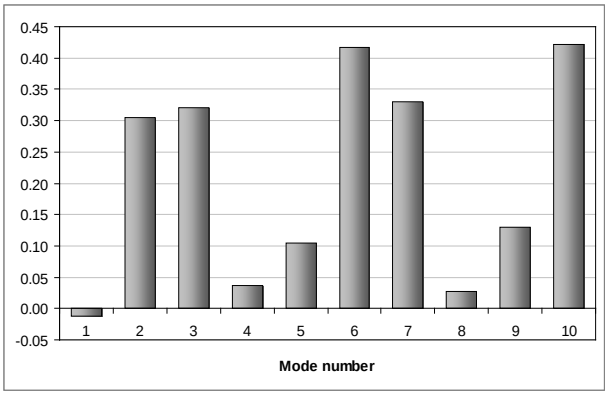


*(b)*

*Figure 3. (a) Frequency shift curves and (b) RFSs for the double-clamped beam damaged at x=254 mm*

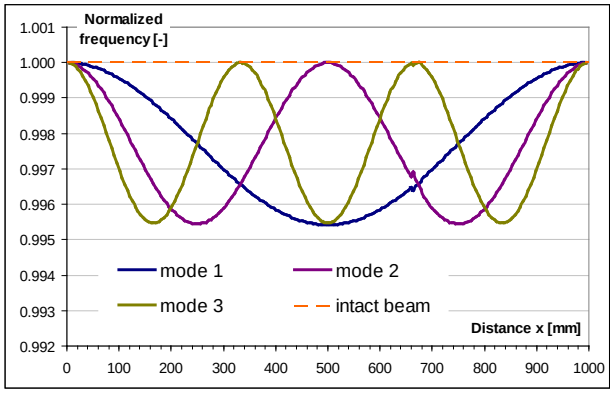


*(a)*

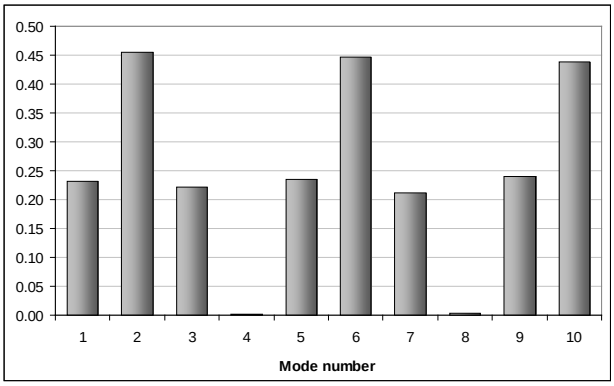


*(b)*

*Figure 4. (a) Frequency shift curves and (b) RFSs for the simply supported beam damaged at x=254 mm*

Analyzing the frequencies of the damaged beams in figures 2 - 4, the curves show that the crack position definitely determines the shift value. Furthermore, it can be observed that, for some modes and locations (e.g. mode 2 and 3 for the cantilever beam at 150 mm and 225 mm respectively), the frequency of the damaged beam exceeds the frequency of the healthy beam. In earlier research, [11-12] we have proved that it happens because the mass loss has a more important effect on the natural frequency as the stiffness decreases. We have also derived the relation for the frequency shift, which is:

$$f_{i-D}(x) = f_{i-U}\cdot\left\{1+\frac{\sqrt{m}-\sqrt{m-4\Delta m}}{\sqrt{m-4\Delta m}}\left[\bar{w}_i(x)\right]^2\right\}- \\ -f_{i-U}\cdot\left\{\frac{\sqrt{\delta_{D\max}}-\sqrt{\delta_{U\max}}}{\sqrt{\delta_{D\max}}}\left[\bar{w}_i''(x)\right]^2\right\} \quad (1)$$

where $f_{i-U}$ and $f_{i-D}$ are the frequencies of the intact and damaged beam, $m$ is the beam mass, $\Delta m$ is the decrease in mass due to damage, $\delta_{U\max}$ and $\delta_{D\max}$ are the highest deflections achieved in mode one for the intact and damaged beam and $\bar{w}_i(x)$ respectively $\bar{w}''_i(x)$ are the mode shape and curvature for the $i^{th}$ vibration mode.

The relative frequency shift curves (RFS) plotted in concordance to Eq. (1) are quite similar with those achieved from FEA, demonstrating that the databases for the prediction of frequencies in beams with open cracks can be designed using this mathematical relation. Obviously, for a breathing crack the mass loss is inexistent, thus the term defining the mass drop in Eq. (1) is suppressed.

Reviewing again Fig. 2(a) to (c) with focus on the frequency changes in different locations, clearly results that patterns characterizing the position of the crack on the beam can be defined from the relative frequency shifts that are:

$$\Delta\bar{f}_i = \frac{f_{i-U}-f_{i-D}}{f_{i-U}}\cdot 100\ [\%] \quad (2)$$

In fact, a sequence of several relative frequency shifts ($i=1\ldots n$) for a given location constitutes the damage indicator for that location. The higher the number of modes involved, the higher the damage assessment precision is. Graphs from Fig. 2(d) to (f) present the damage indicator for the open crack depth $a_3$=1.25 mm located at distance $x$=254 mm from the left beam end. Ten RSFs (i.e. ten vibration modes) are taken for each analyzed beam. The damage indicators in terms of RFS are derivable from numerical simulations or analytically from Eq. (1) and (2). Introducing the accomplished values in the databases, a link between damage depth and location on one side and the corresponding RFSs on the other side is achieved. The complete data is centralized in the three databases, resulting in a vector with $m$ rows and $n\cdot p$ columns. The value of m represents the number of considered vibration modes (10 in this case) and $n$ the number of damage positions multiplied with $p$, which is the number of depth levels (around 200·8=1600 in this analysis). Selected samples, from the database designed for the beam fixed at the left end and free on the right one for damage depth $a_3$=1.25 mm, is presented in Table 1.

Because the structure is asymmetrical, each location has associated an individual damage indicator. In contrast, for symmetric structures the half number of damage indicators is necessary, due to mirroring. The bars depicted in Fig. 2(d) have amplitudes defined using the values indicated for the damage located at position $x$ = 254 mm in Table 1. Dissimilar, for symmetric structures the mirrored locations have the same RFSs, i.e. the values in the sequence representing the damage indicator for both locations are similar.

*Table 1. Relative frequency shifts for the database portion corresponding to the cantilever beam with damage depth $a_3$*

| Mode nr. | Damage position $x$ [mm] | | | | | | | | | | | | |
|---|---|---|---|---|---|---|---|---|---|---|---|---|---|
| | 6 | 9 | 13 | … | **254** | 262 | … | 658 | 667 | … | 975 | 980 | 998 |
| | Damage index $n$ for $p = 3$ | | | | | | | | | | | | |
| | *1* | *2* | *3* | … | ***34*** | *35* | … | *109* | *110* | … | *n-2* | *n-1* | *n* |
| 1 | 0.9926 | 0.9836 | 0.9726 | … | **0.4313** | 0.4171 | … | -0.001 | -0.005 | … | -0.097 | -0.0987 | -0.1037 |
| 2 | 0.9448 | 0.9175 | 0.8819 | … | **0.0004** | 0.0090 | … | 0.3507 | 0.3343 | … | -0.081 | -0.085 | -0.101 |
| 3 | 0.9023 | 0.8583 | 0.8023 | … | **0.2944** | 0.3157 | … | 0.4580 | 0.4809 | … | -0.067 | -0.074 | -0.101 |
| 4 | 0.8616 | 0.8020 | 0.7276 | … | **0.3283** | 0.3015 | … | 0.0124 | 0.0329 | … | -0.054 | -0.063 | -0.099 |
| 5 | 0.8194 | 0.7460 | 0.6551 | … | **0.0425** | 0.0174 | … | 0.2765 | 0.2197 | … | -0.042 | -0.053 | -0.098 |
| 6 | 0.7789 | 0.6932 | 0.5880 | … | **0.0876** | 0.1419 | … | 0.3681 | 0.4115 | … | -0.028 | -0.043 | -0.097 |
| 7 | 0.7406 | 0.6428 | 0.5251 | … | **0.4052** | 0.4371 | … | 0.0013 | 0.0281 | … | -0.014 | -0.032 | -0.096 |
| 8 | 0.7017 | 0.5948 | 0.4666 | … | **0.3477** | 0.2723 | … | 0.3137 | 0.2224 | … | 0.0004 | -0.022 | -0.095 |
| 9 | 0.6665 | 0.5495 | 0.4123 | … | **0.0380** | 0.0025 | … | 0.3351 | 0.4079 | … | 0.0178 | -0.010 | -0.094 |
| 10 | 0.6345 | 0.5088 | 0.3636 | ⋯ | **0.1011** | 0.2012 | ⋯ | -0.001 | 0.0292 | ⋯ | 0.0372 | 0.0024 | -0.093 |

The main idea of the damage assessment method introduced here is to find the indexes n and p for which measured data best fits the RFS sequence in the database. In this way the damage location $x$ and depth $a$ are achieved. Another version of the method, described in [13], consists in normalizing the values in the database by the highest value in the column. In this way the database dimension is reduced by the suppression of the depth influence. As a consequence, just the damage location is found.

## 3. Robustness test for the proposed dissimilarity estimators

According to the presented background, the employment of dissimilarity estimators in the damage assessment method is required. In this section we analyze three estimators: the Minkowski distance, the Histogram intersection and the Kullback-Leibler divergence. The aim of the study is to find out the dissimilarity estimator which best indicates the damage location and severity, even in the presence of noise in the time-domain signals acquired in situ significant. In all cases the algorithm is resumed in finding the vector contained in one of the databases that best fit the RFSs attained from measurements. This is achieved if the distance between the elements of the measured RFS vector and that of a target vector, existent in one of the databases, is minimal. Hence the sum of elements of the error vector gets the lowest value. Fig. 3 illustrates this undertaking.

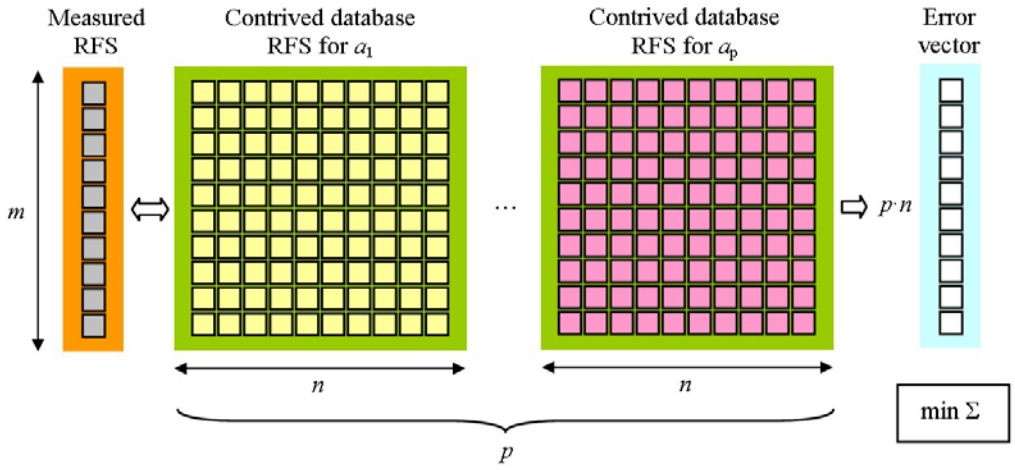


*Figure 3. Best Relative Frequency Shift fit analysis*

For the dissimilarity test, the bin-by-bin approach is adequate since the compared natural frequency pairs must have the same order [14-16]. The reference vector is obtained from measurement results, and reflects the RFS of ten bending modes. Because the reference vector has 10 elements (m in the general case), $i$=1..10. From here on, this vector is denoted $\Psi$:[$\Psi_1$ .. $\Psi_i$ .. $\Psi_{10}$]$^T$. It is compared with the $p \cdot n$ vectors of the $p$ databases, involving RFS derived for the specific boundary conditions. Such vector is denoted as $\Phi_{p\text{-}n}$:[$\Phi_{1xp\text{-}n}$ .. $\Phi_{ixp\text{-}n}$ .. $\Phi_{10xp\text{-}n}$]$^T$ , where $p$-$n$ is the index defining the damage severity and position. It is obtained by concatenating the severity index $k$=1..$p$ and the position index $j$=1..$n$. In the analysis presented in this section $p$=6 and $n$ involves around 200 locations along the beam (individually chosen in respect to the support types).

The Minkowski distance is a generalization of both the Euclidean distance and the Manhattan distance. In the general case, it is expressed as:

$$d_{Lr}(\Psi, \Phi_{p-n}) = \left[ \sum_{i=1}^{10} \left| \Psi_i - \Phi_{ixp-n} \right|^r \right]^{\frac{1}{r}} \qquad (3)$$

The comparison is individually performed for all p-n cases, aiming to find the lowest value of $d_{Lr}$. The Manhattan distance results from Eq. (3) for $r$ = 1 as well as the Euclidean distance for $r$ = 2. The minimum becomes easy to find by representing all values in a graph, in this way locating the damage (defined by the index of $n$) and estimating its severity (defined by the index of $p$). Fig. 4. illustrates the particular cases of a cantilever beam with an open crack of depth $a_3$ = 1.65 mm, located at the distance $x$ = 834 mm from the fixed end. The frequencies are assumed to be achieved with good accuracy, producing to the RFSs an error less than ±2%. A zoom on the area of interest from in the above mentioned graph is presented in Fig. 5(a) in order to make possible a comparison with the Minkowski distance that was derived for errors up to ±15% and depicted in Fig. 5(b).

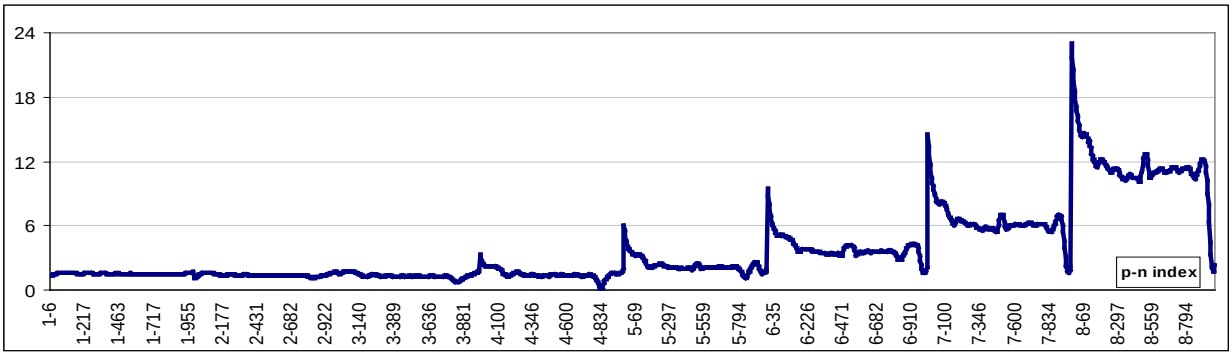


*Figure 4. The Minkowski distance for a cantilever beam with an open crack of depth $a_4$ = 1.65 mm and located at x= 834 mm*

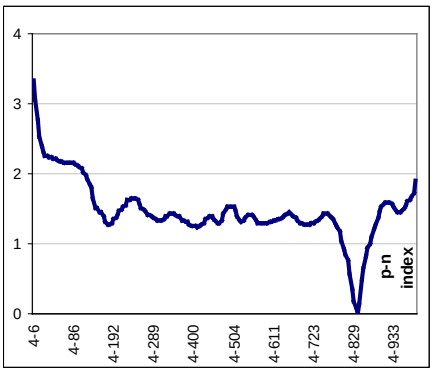


*(a) Precise damage assessment (x = 834 mm from the fixed end)*

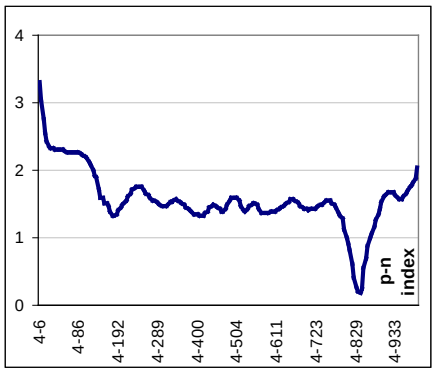


*(b) Precise damage assessment (x = 834 mm from the fixed end)*

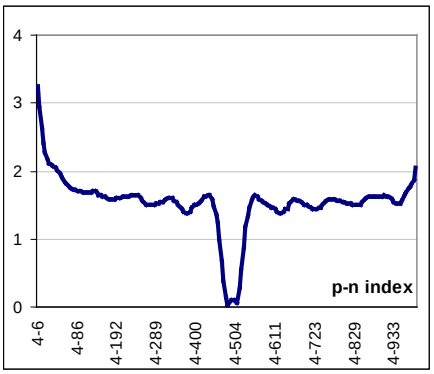


*(c) Ambiguous damage assessment (x = 491 mm from the fixed end)*

*Figure 5. The Minkowski distance for a cantilever beam with an open crack of depth $a_4$ = 1.65 mm (zoom on the region representing the fourth damage depth level)*

From Fig. 5(a) and (b) clearly results that precise damage assessment is possible even if the frequencies are acquired with noise. In our study we found out that a RFS alteration of 15% still allows a precise damage assessment if the damage depth is close to one of the values contained in the databases. On the other hand, even in the case of accurate frequency evaluation, for the cantilever, a segment located around the beam mid-span provides quite similar $d_{Lr}$ values, thus just the damage region can be found. Even in this case the damage severity precisely results, this fact being illustrated in Fig. 5(c). Note that all presented results were attained for order $r$ = 2, i.e. employing the Euclidean distance. Analyzes performed for other orders (1, 3 and 4) did not dramatically affect the results, hence the precision of the damage assessment method being not altered.

If the assessment process is possible for damage with the depth that falls between two existing depth levels in the database is also of interest. For this issue we created virtual damages with the depth framed by the levels $a_3$ and $a_4$. In this case, simulations have shown that the location is precisely pointed out, but two possible depths are indicated. Fig. 6(a) illustrates this aspect, for the damage location $x$ = 834 mm and the damage depth $a$ = 138 mm. In the beam mid-span, the location is again not precisely identifiable, the crack position is supposed to be in a region extended on approximately 0.1$L$. The damage severity is correctly indicated between 1.25 and 1.65 mm. However, the assessment process indicates by enough precision the crack location and the progress.

It has to be mentioned that we performed simulations for a wide range of damage parameters, meaning depth until a cross-section reduction of 67% is achieved and very dense positions on the beam, and can state that the conclusions above presented are valid for all possible damage scenarios.

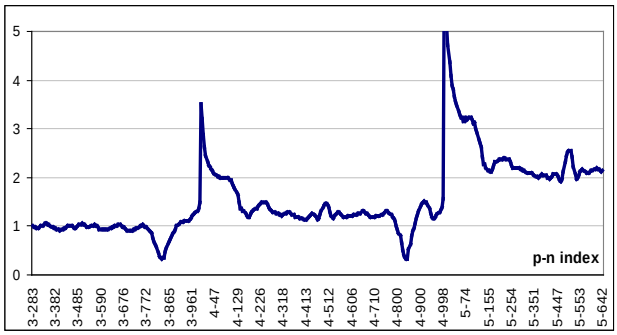


*(a) Damage assessment for x = 834 mm*

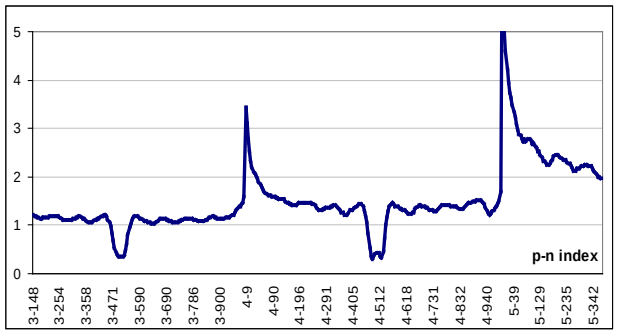


*(b) Damage assessment for x = 491 mm*

*Figure 6. The Minkowski distance for a cantilever beam with an open crack of depth a = 1.38 mm (zoom on the region representing the damage depth levels $a_3$ to $a_5$)*

For the simply supported and double-clamped beams, based on the symmetry of the structure, it is sufficient to analyze a half-beam, but in these cases two damage locations are predicted. The study revealed that the severity of a crack located near the pinned end of the simply supported beam is hard to be estimated. It happens because the frequencies of all modes insignificantly shift for damages placed very close to the pinned end.

In Fig. 7(a) the values of the Minkowski distance are plotted for a severe damage ($a_4$ = 1.65 mm) located at $x$ = 11 mm from one beam end. One can observe the numerous points near the abscissa, hence possible correct severity indicators. Remark that all these points precisely indicate the damage position. In contrast, for damages which are not in the proximity of the pinned ends, the position and severity are easily contrived, see Fig. 7(b).

Analyzing the double-clamped beam with an open crack we found out that the damage severity and location can be identified without doubt, the Minkowski distance precisely indicating the minima, irrespective to the damage size or position,

as exemplified in Fig. 8(a) for a crack placed close to the fixed end, and in Fig. 8(b) for a crack near to the beam's mid-span.

The conclusions drown by reviewing Fig. 4 to 8 take into consideration a large number of possible damage cases (position and depth), having a large degree of generality. It was shown that the Minkowski distance is a reliable damage indicator.

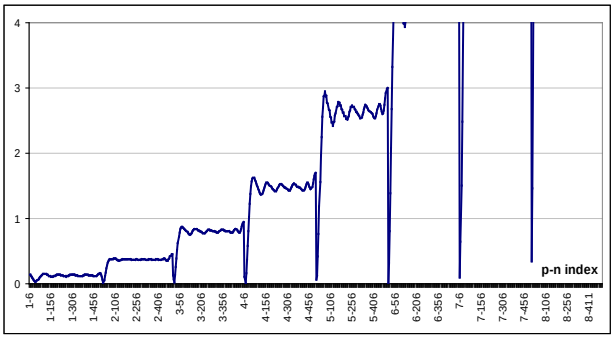


*(a) Diagram for the damage at distance x = 11 mm*

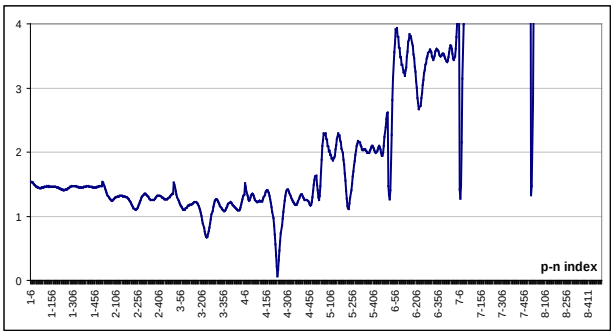


*(b) Diagram for the damage at distance x = 201 mm*

*Figure 7. The Minkowski distance for a simply supported beam with an open crack of depth $a_4$ = 1.65 mm*

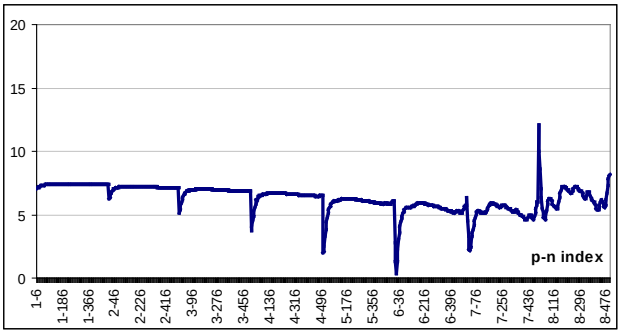


*(a) Diagram for the damage located at distance x = 16 mm, and having the depth $a_6$ = 2.5 mm*

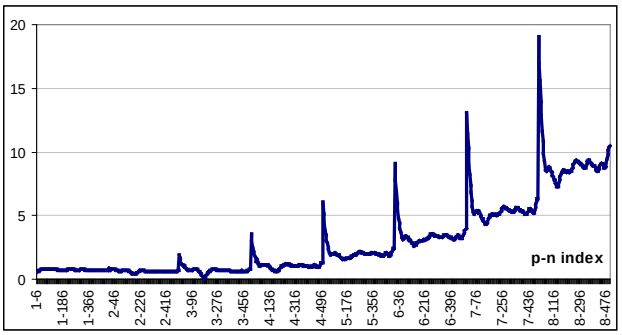


*(b) Diagram for the damage located at distance x = 181 mm, and having the depth $a_3$ = 1.25 mm*

*Figure 8. The Minkowski distance for a double-clamped beam with an open crack*

The normalized histogram intersection estimates the similarity between two histograms or vectors, indicating the perfect fit by returning the unit value. It is expressed:

$$d_{\text{int}}(\Psi,\Phi_{p-n}) = \frac{\sum_{i=1}^{10} \min\left(\Psi_i, \Phi_{ixp-n}\right)}{\sum_{i=1}^{10} \Psi_i} \qquad (4)$$

The distance is calculated for the *p·n* scenarios for the cantilever beam. Fig. 9 exemplifies the case of a damage with depth 0.85 mm, which is located at 500 mm from the fixed end.

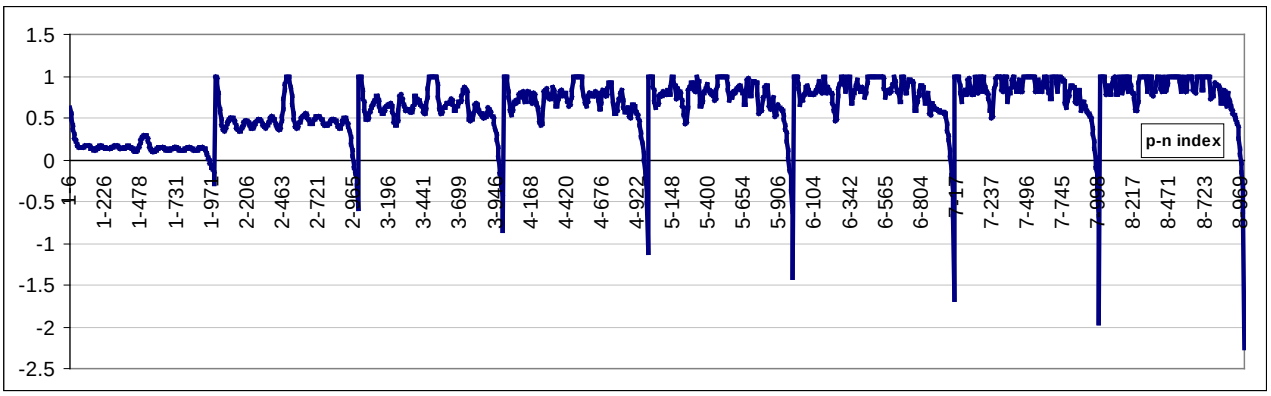


*Figure 9. The normalized histogram intersection for a clamped beam with an open crack located at distance x = 500 mm and having the depth $a_2$ = 0.85 mm*

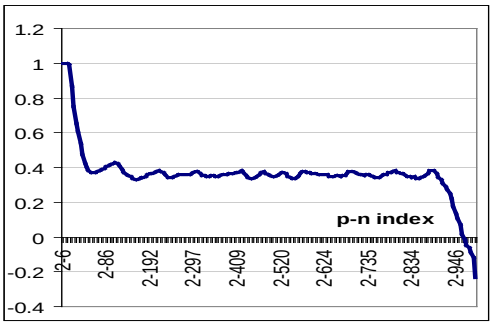


*(a) Diagram for damage at x = 17 mm*

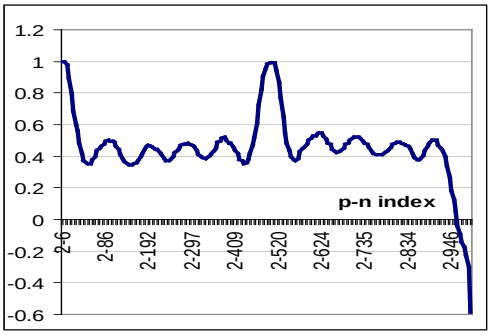


*(b) Diagram for damage at x = 500 mm*

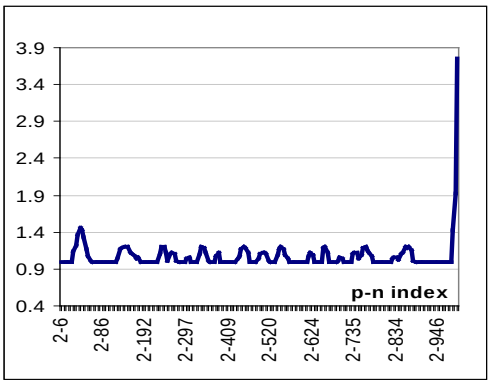


*(c) Diagram for damage at x = 971 mm*

*Figure 10. The normalized histogram intersection for a clamped beam with an open crack having the depth $a_2$ = 0.85 mm*

The normalization is requested because the sum in the nominator increases with the increasing of the damage depth, and so the best fit is not any more indicated by $d_{int}$ = 1. Alternatively, for all damage depths a separate analysis should be made, but in this case the assessment of cracks with depth different from that contained in the database is not possible. It is worth to mention that the analysis was performed for errors up to ±2% in the RFSs, thus the indicator value showing the best fit will lightly differ from the unit.

Having a look on the graphs in Fig. 10, one can observe that the damage is precisely located for any position on the beam, excepting the fixed respectively free end, for these last positions only the damaged region being indicated. However, in the particular case of cantilever beams, damage in the proximity of the fixed end will always be indicated.

The Kullback-Leibler (KL) Divergence, which employs the properties of the logarithmic function, is described by:

$$d_{\log}(\Psi, \Phi_{p-n}) = \sum_{i=1}^{10} \Psi_i \log \frac{\Psi_i}{\Phi_{ixp-n}} \qquad (5)$$

In this approach, the vector $\Psi$ representing the "true" data (RFSs derived from measurements) is compared with all $p \cdot n$ vectors $\Phi$ contrived by means of FEA or calculus included in the database. The aim is to find the lowest value in the attained $d_{log}$ sequence, indicating the best vectors fitting. Obviously, if two vectors are identical the result is null. As in the case of the histogram intersection, the weak point is the existence of negative values, both in data attained from measurements as well as in the database.

Since the log function does not handle negative values, the alternative is to use the “zero” value for all non-positive data. As the negative RFSs values are small in absolute value, an insignificant influence of this approach upon the results is

expected. Fig. 11 depicts the KL divergence for a severe damage, depth $a_6$ = 2.5 mm, located at $x$ = 674 mm away from the fixed end. In this case, the crack is recognized with precision, even for RFSs attained from noisy vibration signals.

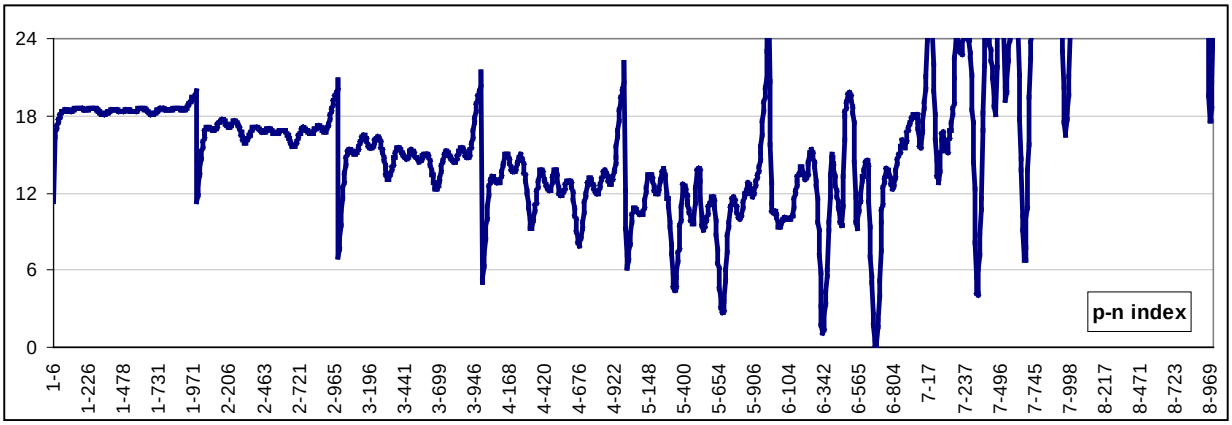


*Figure 11. The KL divergence for a clamped beam with an open crack located at x = 674 mm and having the depth $a_6$ = 2.5 mm*

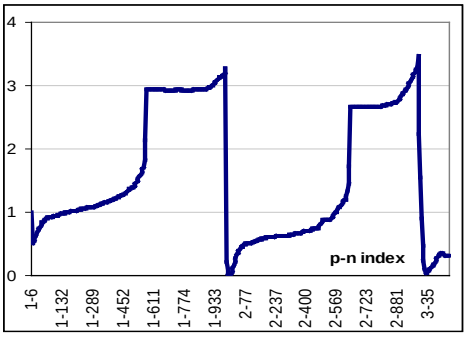


*(a) Diagram for damage at x = 17 mm*

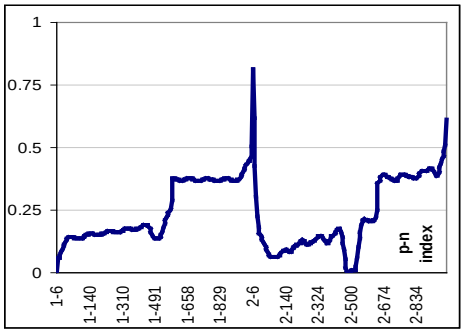


*(b) Diagram for damage at x = 494 mm*

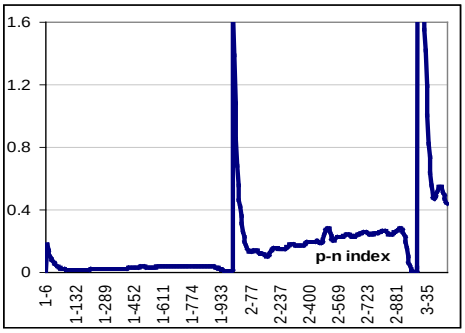


*(c) Diagram for damage at x = 971 mm*

*Figure 12. The KL divergence for a clamped beam with an open crack having the depth $a_2$ = 0.85 mm*

From the numerous simulations performed, we found out that the assessment of damage in the early state becomes difficult, even if advanced frequency estimation techniques are used [17-19]. Moreover, if the crack is located near the fixed or free beam ends, a clear severity prediction is not possible. This is exemplified in Fig. 12(a) and (c) for damage located at 17 respectively 971 mm from the fixed end. Also, Fig. 12(b) presents a region where the damage position is not clearly defined, namely the beam mid-span.

## 4. Conclusion

In this paper a systematic study regarding the effectiveness of three dissimilarity estimators with application in damage detection is presented. These dissimilarity estimators, namely the Minkowski distance, the histogram intersection and the Kullback-Leibler divergence, were employed to find the best fit between the frequency changes achieved by measurements and from database, containing reference values for all possible damage scenarios.

The database of frequencies has been accomplished analytically and by means of FEA. In the analytical approach, a mathematical relation contrived by the authors predicts frequency changes due to the cracks. Since it makes use of the natural frequencies, mode shapes and curvatures of the healthy beam, obviously this relation can be performed for beams with any boundary conditions. In respect to the considered support types, characterizing damages places successively along the beam in around 200 locations and with eight levels of dept, three databases have been resulted. The validation of the mathematical relation was made comparing its results to those obtained by FEA. Note that a multimodal frequency

analysis was performed, making use of the property of the low frequencies, which better indicate the damage depth, and the higher frequencies, which are more sensitive to the location. In order to frame the database values in a reasonable range, we used the relative frequency shifts.

Based on the results and presented discussions it can be determined that even if the real damage depth is not contained in the database, the damage location and position can be evaluated by enough precision.

**Acknowledgements**

The work has been funded by the Sectoral Operational Programme Human Resources Development 2007-2013 of the Ministry of European Funds through the Financial Agreement POSDRU/159/1.5/S/132395.

**References**

[1]. Trendafilova, I. (2011). A Method for Vibration-Based Structural Interrogation and Health Monitoring Based on Signal Cross-Correlation, Journal of Physics: Conference Series, vol. 305, no. 1, article 012005.

[2]. Doebling, S. W., Farrar, C. R. and Prime M. B. (1998). *A summary review of vibration-based damage identification methods*, Shock and Vibration Digest, vol. 30, no. 2, pp. 91-105.

[3]. Gillich, G.-R. and Praisach, Z.-I. (2013). *Detection and quantitative assessment of damages in beam structures using frequency and stiffness changes*, Key Engineering Materials, vol. 569-570, pp. 1013-1020.

[4]. Mottershead, J. E. and Friswell, M. I. (1993) *Model updating in structural dynamics: A survey*, Journal of Sound and Vibration, vol. 167, no. 2, pp. 347-375.

[5]. Gillich, G. R., Birdeanu, E. D., Gillich, N., Amariei, D., Iancu, V. and Jurcau, C. S. (2009). *Detection of damages in simple elements*, Annals of DAAAM for 2009 & Proceedings of the 20th International DAAAM Symposium, Book Series: Annals of DAAAM and Proceedings, vol. 20, pp. 623-624.

[6]. Fritzen, C. P. and Jennewein, D. (1998). *Damage detection based on model updating methods*, Mechanical Systems and Signal Processing, vol. 12, no. 1, pp. 163-186.

[7]. Kullaa, J. (2004). *Structural health monitoring under variable environmental or operational conditions*, Proceedings of the second European Workshop on Structural Health Monitoring, pp. 1262–1269.

[8]. Elshafey, A. A., Marzouk, H. and Haddara, M. R. (2011). *Experimental Damage Identification Using Modified Mode Shape Difference*, Journal of Marine Science and Application, vol. 10, pp.150-155.

[9]. Radzieński, M. and Krawczuk, M. (2009). *Experimental Verification and Comparison of Mode Shape-based Damage Detection Methods*, Journal of Physics: Conference Series, vol. 181, art. 012067.

[10]. Pandy, A. K., Biswas, M. and Samman, M. M. (1991). *Damage detection from changes in curvature mode shapes*, Journal of Sound and Vibration, vol. 145, no. 2, pp. 321–332.

[11]. Praisach, Z. I., Gillich, G. R. and Birdeanu, E. D. (2010). *Considerations on Natural Frequency Changes in Damaged Cantilever Beams Using FEM*, 3rd WSEAS International Conference on Engineering Mechanics, Structures, Engineering Geology/International Conference on Geography and Geology Corfu Island, Greece, pp. 214-219.

[12]. Gillich, G.-R., Praisach, Z. I., Furdui, H., Ntakpe, J. L., Minda, A. A. (2014). *Evaluation of loss of mass due to corrosion using vibration-based methods*, Applied Mechanics and Materials, vol. 658, pp. 77-82.

[13]. Gillich, G.-R., Praisach, Z.-I. and Negru, I. (2012) *Damages influence on dynamic behaviour of composite structures reinforced with continuous fibers*, Materiale Plastice, vol. 49, no. 3, pp. 186-191.

[14]. Minda, P.F., Praisach, Z.-I., Gillich, N., Minda, A.A., Gillich, G.-R. (2013). *On the efficiency of different dissimilarity estimators used in damage detection*, Romanian Journal of Acoustics and Vibration, vol. 10, no. 1, pp. 15-18.

[15]. Chioncel, C., Babescu, M., Chioncel, P., Gillich, N. and Gillich, G.-R. (2007). *Speed Control Method for Asynchronous Motor*, Annals of DAAAM for 2007 & Proceedings of the 18th International DAAM Symposium: Intelligent manufacturing & Automation, vol. 18, pp. 137-138.

[16]. Cheung, A., Cabrera, C., Sarabandi, P., Nair, K. K., Kiremidjian, A. and Wenzel, H. (2008). *The application of statistical pattern recognition methods for damage detection to field data*, Smart Materials and Structures, vol. 17, no. 6, art. 065023.

[17]. Gillich, G.-R., Frunzaverde, D., Gillich, N. and Amariei, D. (2010). *The use of virtual instruments in engineering education*, Elsevier Sciences Direct: Procedia Social and Behavioral Sciences, vol. 2, pp. 3806–3810.

[18]. Chioncel, C. P., Gillich, N., Tirian, G. O. and Ntakpe, J. L. (2015) *Limits of the Discrete Fourier Transform in Exact Identifying of the Vibrations Frequency*, Romanian Journal of Acoustics and Vibration, vol. 12, no. 2, pp. 20-28.

[19]. Gillich, G.-R., Nuno, Maia, M.M., Mituletu, I.-C., Praisach, Z.-I., Tufoi, M., and Negru, I. (2015). *Early Structural damage Assessment by Using an Improved Frequency Evaluation Algorithm*, Latin American Journal of Solid and Structures, vol.12, no. 12, pp. 2311-2329.